Poly(3-hexylthiophene)/Multiwalled Carbon Hybrid Coaxial Nanotubes: Nanoscale Rectification and Photovoltaic Characteristics

Kihyun Kim,[†] Ji Won Shin,[†] Yong Baek Lee,[†] Mi Yeon Cho,[†] Suk Ho Lee,[†] Dong Hyuk Park,[†] Dong Kyu Jang,[‡] Cheol Jin Lee,[‡] and Jinsoo Joo[†,*]

[†]Department of Physics and Hybrid Nanostructure Research Lab, Korea University, Seoul 136-713, Korea, and [‡]School of Electrical Engineering and Department of Micro/Nano Systems, Korea University, Seoul 136-713, Korea

ABSTRACT We fabricate hybrid coaxial nanotubes (NTs) of multiwalled carbon nanotubes (MWCNTs) coated with light-emitting poly(3-hexylthiophene) (P3HT). The *p*-type P3HT material with a thickness of ~20 nm is electrochemically deposited onto the surface of the MWCNT. The formation of hybrid coaxial NTs of the P3HT/MWCNT is confirmed by a transmission electron microscope, FT-IR, and Raman spectra. The optical and structural properties of the hybrid NTs are characterized using ultraviolet and visible absorption, Raman, and photoluminescence (PL) spectra where, it is shown that the PL intensity of the P3HT materials decreases after the hybridization with the MWCNTs. The current−voltage (*I*−*V*) characteristics of the outer P3HT single NT show the semiconducting behavior, while ohmic behavior is observed for the inner single MWCNT. The *I*−*V* characteristics of the hybrid junction between the outer P3HT NT and the inner MWCNT, for the hybrid single NT, exhibit the characteristics of a diode (*i.e.*, rectification), whose efficiency is clearly enhanced with light irradiation. The rectification effect of the hybrid single NT has been analyzed in terms of charge tunneling models. The quasi-photovoltaic effect is also observed at low bias for the P3HT/MWCNT hybrid single NT.

KEYWORDS: hybrid nanomaterial · multiwalled carbon nanotube · poly(3-hexylthiophene) · rectification · photovoltaic effect · nano characterization

Organic-based optoelectronic devices, such as organic light emitting diodes (OLEDs) and organic thin film transistors (OTFTs), have been developed for flexible display units.[1] Organic photodiodes and phototransistors are fabricated by using photosensitive π-conjugated organic materials,[2,3] and the photovoltaic (PV) effects of these materials have been also intensively studied and applied to inexpensive and renewable energy sources.[4,5]

Charge recombination and dissociation in the p−n junctions of semiconductors can provide various applications such as diode lasers, LEDs, photodetectors, and PV cells. With the rapid development of nanotechnology, nanoscale p−n junctions have been investigated by using low-dimensional nanostructures such as carbon nanotubes (CNTs) and inorganic or organic semiconducting nanowires (NWs).[6−9] Huang and co-workers fabricated integrated nanoscale field-effect transistor (FET) arrays and logic gates using the crossed Si NW p−n junctions and junction arrays.[6] Lee and co-workers reported the PV effect of an individual single-walled carbon nanotube p−n junction diode through electrostatic doping using a pair of split gate electrodes.[7,8] A single strand of coaxial Si NW with p-type/intrinsic/n-type (PIN) doped semiconductor structure has been experimentally realized as a nanoscale electronic power source.[9]

Charge transport properties in coaxial-type p−n junction NWs have recently been studied by Lieber's and other groups.[9−11] Dissociated charges from photogenerated excitons in the coaxial p−n junction NWs are separated in the radial direction of the NW, which can be easily transported to electrodes through an equipotential surface formed along the axial direction in the NW.[9−11] Therefore, the charge transport in coaxial p−n junction NWs can be improved, compared with that of the serial type p−n junction NWs.[12] In addition, the high aspect ratio of the coaxial p−n junction NWs allows a large junction area for effective optical absorption.[10,12] The coaxial p−n junction NW is a promising nanostructure for nanoscale optoelectronics in terms of charge transport and efficient optical absorption.[9−12]

CNTs have been studied in the fields of fundamental nanoscience research and applications because of their excellent electrical, thermal, and mechanical properties

*Address correspondence to jjoo@korea.ac.kr.

Received for review March 2, 2010 and accepted June 03, 2010.

Published online June 9, 2010.
10.1021/nn100427f

with well-defined nanostructures. CNTs can be a direct path of charge transport to the electrode and can be used as the electron acceptor (*i.e.*, relative *n*-type characteristics compared with *p*-type π-conjugated organic materials) in organic-based optoelectronic devices.[13−15] π-Conjugated light-emitting poly(3-hexylthiophene) (P3HT) materials with a broad optical absorption band, have a crystalline structure and can be soluble in common organic solvents, which contribute to their use as active *p*-type material for organic-based optoelectronics such as OLEDs, OTFTs, and organic photovoltaic (OPV) cells.[16−20] OPV cells using electrochemically deposited doped-P3HT film showed the fill factor (FF) of ~0.65 and power conversion efficiency of ~1%.[21]

In this study, we report on the fabrication and the photoresponsive electrical characteristics of the hybrid coaxial nanotube (NT), consisting of a multiwalled carbon nanotube (MWCNT) coated with the light-emitting P3HT material. The *p*-type P3HT material is directly deposited onto the MWCNT surface using an electrochemical polymerization method. Using electrical contacts at four different positions on an isolated single strand of P3HT/MWCNT hybrid NTs, the current−voltage (*I*−*V*) characteristic curves have been measured and analyzed. The *I*−*V* characteristics of the hybrid junction between the P3HT NT and the MWCNT in the hybrid single NT show the rectification behavior, and this is enhanced by light irradiation, because of the contribution of the photogenerated charges at the junction interface. The quasi-photovoltaic effect is also observed in the P3HT/MWCNT hybrid single NT.

RESULTS AND DISCUSSION

Fabrication of Coaxial-type P3HT/MWCNT Hybrid NTs and of a Single NT Device. The doped Si substrate with the as-grown MWCNTs synthesized through the thermal chemical vapor deposition (CVD) method is attached on the stainless steel working electrode, as shown in Figure 1a. The P3HT layer with a thickness of ~20 nm is directly deposited onto the surface of the MWCNTs using an electrochemical polymerization method. The electrolyte for the electrochemical polymerization consists of 3-hexylthiophene (3-HT) monomers, 1-butyl-3-methylimidazolium hexafluorophosphate ($BMIMPF_6$) ionic liquid, and anhydrous acetonitrile (CH_3CN) as the solvent. For the polymerization of the 3-HT monomers, a constant voltage of 4.3 V is applied for 90 s to obtain uniform P3HT layer onto the MWCNT, and the measured current density between electodes is 1.6 mA/cm^2.[22] It is difficult to obtain a thicker P3HT layer on the MWCNT in the form of an isolated single hybrid NT, because of the narrow space between MWCNTs.

To study the *I*−*V* characteristics with and without light illumination and the fabrication of the nanoscale device using the single strand of P3HT/MWCNT hybrid NT, an E-beam lithography technique is employed for electrical contacts of Au/Ti electrodes. To contact the

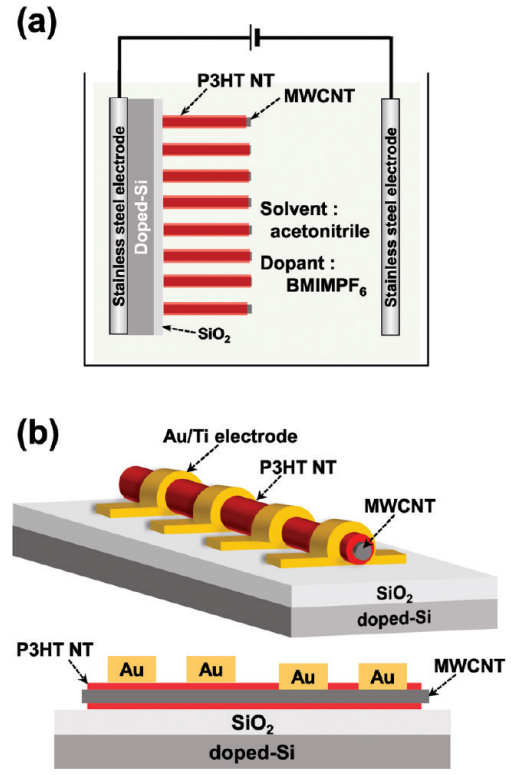

Figure 1. (a) Schematic illustration of electrochemical deposition of the P3HT onto the MWCNT surface. (b) Schematic diagram of nanoscale device using a single strand of the P3HT/MWCNT hybrid NT with four-probe Au/Ti electrodes (top). Cross sectional view of nanoscale device using a single strand of the P3HT/MWCNT hybrid NT with four-probe Au/Ti electrodes (bottom).

Au/Ti electrode on the MWCNT part, the P3HT layer wrapping on the MWCNT is partially etched by using a xylene ($C_6H_4(CH_3)_2$) solution after development of the E-beam resist exposed by E-beam lithography. Figure 1b shows a schematic illustration of the four-probe electrodes on the P3HT/MWCNT hybrid single NT. In the single strand of P3HT/MWCNT hybrid NT, two Au/Ti electrodes are contacted on the outer P3HT single NT, while another two Au/Ti electrodes are contacted on the inner single MWCNT through the partial etching of the P3HT. This configuration of electrodes is confirmed by SEM images and their magnification image.

Structural and Optical Properties. The formation and surface morphology of the coaxial P3HT/MWCNT hybrid NTs are investigated using HR-TEM and SEM images, as shown in Figure 2. The MWCNTs have outer diameters of 10−30 nm and a wall thickness of 2−8 nm, as shown in Figure 2a. Figure 2b shows a HR-TEM image of the P3HT/MWCNT hybrid NT. The total diameter of the hybrid NT is ~60 nm. The thickness of the P3HT layer deposited onto the MWCNT is ~20 ± 10 nm with applied bias of 4.3 V, and the formation of the coaxial-type NT of MWCNTs coated with P3HT materials is clearly observed.

Figure 3a shows the Raman spectra of the P3HT NTs, the MWCNTs, and the P3HT/MWCNT hybrid NTs.

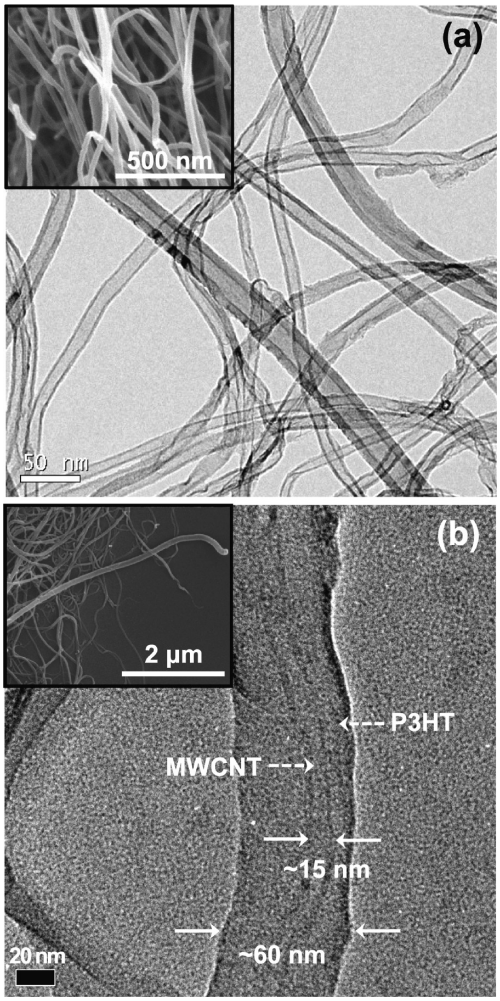

Figure 2. (a) HR-TEM image of the MWCNTs. Inset: SEM image of the MWNCTs. (b) HR-TEM image of the P3HT/MWCNT hybrid NT. Inset: SEM image of the P3HT/MWCNT hybrid NTs.

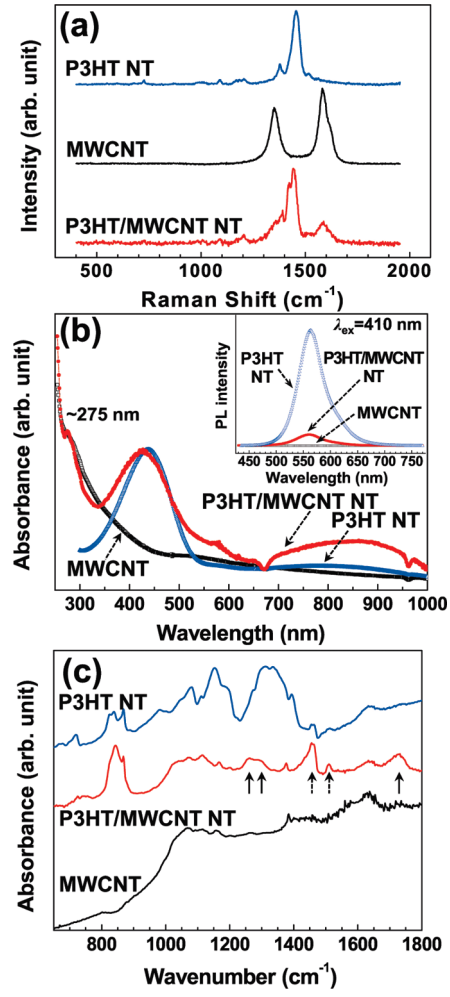

Figure 3. (a) Raman spectra for the P3HT NTs, MWCNTs, and P3HT/MWCNT hybrid NTs. (b) Normalized UV−vis absorption spectra for the P3HT NTs, MWCNTs, and P3HT/MWCNT hybrid NTs. Inset: PL spectra of the NTs. (c) FT-IR spectra for the P3HT NTs, MWCNTs, and P3HT/MWCNT hybrid NTs.

The P3HT NTs are separately synthesized without the MWCNTs through the same electrochemical method (see the Experimental Section). For the P3HT NTs themselves, Raman characteristic peaks for the P3HT material are observed at 1452.4 (±4.0), 1378.9 (±1.1), and 1516.6 (±2.2) cm^{-1}, which correspond to the vibrational mode by $C_\alpha{=}C_\beta$ stretching of the thiophene ring, the $C_\beta{-}C_{\beta'}$ stretching of the thiophene ring, and the $C_{\alpha'}{=}C_{\beta'}$ stretching modes of the thiophene ring, respectively.[23] Two Raman bands are observed at 1351.7 (±1.7) (D-band) and 1584.5 (±2.2) cm^{-1} (G-band) for the MWCNTs.[24] For the P3HT/MWCNT hybrid NTs, Raman characteristic peaks corresponding to P3HT and MWCNT materials are simultaneously observed at 1356.9 (±5.8), 1377.0, 1444.4 (±2.3), 1516.0, and 1587.8 (±1.4) cm^{-1}. We observe the slight shift to high wavenumber for the D- and G-bands after the hybridization. The full width at half-maximum (fwhm) for the D- and G-bands of the MWCNT is estimated to be ~52.2 and ~43.4 cm^{-1}, respectively (see Supporting Information). However, the fwhm for the D- and G-bands of the P3HT/MWCNT hybrid NTs is estimated to be ~66.1 and ~47.0 cm^{-1}, respectively, implying the variation of vibration modes of MWCNT due to the hybridization with the P3HT materials. The similar results for the variation of the fwhm of the D- and G-bands of the MWCNT hybridized with poly(L-lactide) material were reported previously.[25,26]

Figure 3b shows normalized UV−vis absorption spectra for the P3HT NTs, the MWCNTs, and the P3HT/MWCNT hybrid NTs. The UV−vis absorption characteristic peak of the MWCNTs is detected at 275 nm.[27] The UV−vis absorption peak of the P3HT NTs is observed at 438 nm corresponding to the $\pi-\pi^*$ transition of the regiorandom P3HT materials.[28] For the P3HT/MWCNT hybrid NTs, the UV−vis absorption characteristic peaks, due to the MWCNT and P3HT materials, are simultaneously observed at 275 and 427 nm, respectively. After the hybridization of the MWCNTs with the P3HT material, the $\pi-\pi^*$ transition peak is shifted from 438 to 427 nm, and the line-width becomes broadened slightly compared with that of the P3HT NTs.[14,29] These might

TABLE 1. Assignments of FT-IR Characteristic Peaks for the P3HT NTs, MWCNTs, and P3HT/MWCNT Hybrid NTs

positions (cm^{-1})	assignments	observation[a] P3HT NTs	MWCNTs	P3HT/MWCNT NTs
721	methyl rock of hexyl group	○	×	○
825	$C_\beta-H$ bending of thiophene ring	○	×	○
867	CH_3 terminal rocking	○	×	○
980	C−S stretching	○	×	○
1081	C−H in phase bending or C═S^+O^-	○	×	○
1261	C−C inter-ring bond stretch	×	×	○
1273	C−C stretching of the C_2-C_2'	○	×	○
1300	C═C stretching	○	×	○
1376	methyl (CH_3) deformation	○	×	○
1392	symmetry and asymmetry bending of OH^- group methyl C−H in phase bending, localized modes for bipolarons	○	○	○
1460	symmetric ring stretching mode	○	×	○
1510	asymmetric ring stretching mode	○	×	○
1633	C═C stretching mode	○	○	○
1731	C═O stretching mode	×	×	○
2584	CH_2 out of phase mode	○	×	○
2923	CH_2 in phase mode	○	×	○
2953	CH_2 asymmetry stretching mode	○	×	○
3444	OH^- stretching mode	○	○	○

[a]Key: (○) observed; (×) not observed.

originate from the formation of the dangling bonds between the P3HT and MWCNTs, which will be discussed in the FT-IR results section. With the hybridization of MWCNTs with the P3HT material, a new broad bipolaron band is observed at ~830 nm. This broad and weak bipolaron band of the P3HT/MWCNT hybrid NTs implies the lightly doped states of the P3HT, which are caused by the electron accepting characteristics due to the MWCNTs (*i.e.*, creation of holes in the P3HT layer).[14,30,31] The PL spectra for the P3HT NTs, the MWCNTs, and the P3HT/MWCNT hybrid NTs are measured under the same experimental conditions, as shown in the inset of Figure 3b. The PL intensity of the P3HT NTs at 560 nm is relatively higher than that of the P3HT/MWCNT hybrid NTs, while the PL is not observed for the MWCNTs. The PL spectrum of the P3HT/MWCNT hybrid NTs is quenched because of the charge transfer effect (*i.e.*, charge dissociation) between the MWCNT and the P3HT materials.[14,31]

The quantum yields (Φ_{QY}'s) for electrochemically synthesized P3HT NTs with the treatment of HF and NaOH solvent to remove the Al_2O_3 template only are measured to be 0.025 and 0.109, respectively (see Supporting Information). The measured Φ_{QY}'s are relatively higher than that of the doped P3HT materials, because of the use of $BMIMPF_6$ ionic liquid providing high ionic conductivities and enhanced lifetimes.[32−34] Ionic liquids such as $BMIMPF_6$ in electrochemical deposition is a new reaction media which can remarkably improve physical and chemical properties of deposited material. From the UV−vis absorption spectrum of the P3HT NTs in Figure 3b, the bipolaron band due to the doping at ~830 nm is not observed, which supports the relative high Φ_{QY} and PL intensity of the electrochemically synthesized P3HT NTs studied here.

Figure 3c compares the FT-IR spectra of the P3HT NTs, the MWCNTs, and the P3HT/MWCNT hybrid NTs. The FT-IR characteristic peaks, corresponding to the P3HT materials, are observed, as shown in Figure 3c. For the P3HT/MWCNT hybrid NTs, the IR characteristic peaks corresponding to the P3HT and the MWCNTs materials are all observed, as listed in Table 1. The intensities of the peaks at 1460 and 1510 cm^{-1} for the P3HT/MWCNT hybrid NTs increase relatively in comparison with those of the P3HT NTs. The intensity ratio (I_{sym}/I_{asym}) of the symmetric ring stretch at 1460 cm^{-1} to the asymmetric stretch at 1510 cm^{-1} indicates the π-conjugation length in the P3HT main chains;[28] the π-conjugation length in the polymer main chains is found to be inversely proportional to the ratio of I_{sym}/I_{asym}. The I_{sym}/I_{asym} for the P3HT NTs and the P3HT/MWCNT hybrid NTs is estimated from the areas by integration of FT-IR peaks at 1460 and 1510 cm^{-1} (see Supporting Information). The estimated ratios of the I_{sym}/I_{asym} are ~3.31 for the P3HT NTs and ~9.34 for the P3HT/MWCNT hybrid NTs, which indicate that the π-conjugation length of the P3HT/MWCNT hybrid NTs is shorter than that of the P3HT NTs. It is also observed that the C═C stretch mode at 1300 cm^{-1} considerably decreases, and the C−C inter-ring bond stretch mode at 1261 cm^{-1} appears as a new characteristic for the P3HT/MWCNT hybrid NTs, as listed in Table 1. A new IR absorption peak at 1731 cm^{-1}, corresponding to the C═O stretch mode such as dangling bonds, is observed after the hybridization of the MWCNT with P3HT materials, which is usually observed for the functionalized CNTs.[35,36] On the basis of the FT-IR results of the P3HT/MWCNT hybrid NTs,

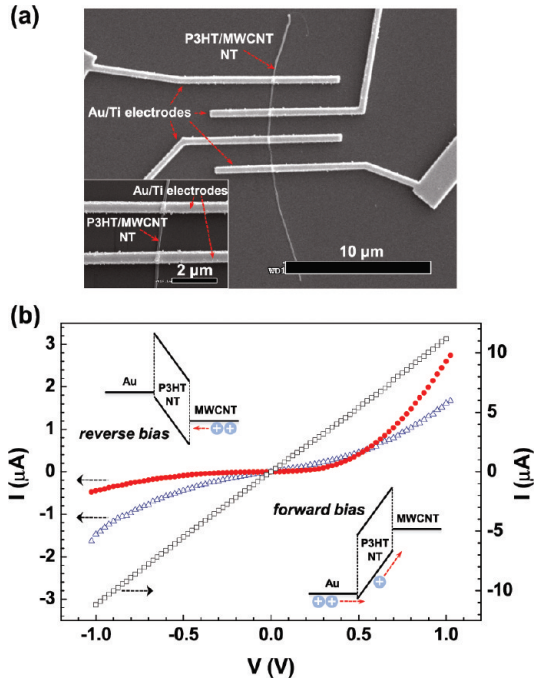

Figure 4. (a) SEM image of a single strand of the P3HT/MWCNT hybrid NT with four-probe electrodes. Inset: magnification of SEM image of a single strand of the P3HT/MWCNT hybrid NT contacted with Au/Ti electrodes. (b) *I*−*V* characteristic curves of a single strand of the P3HT NT (Δ), MWCNT (□), and P3HT/MWCNT hybrid NT (●) measured in the dark condition at room temperature. Top and bottom insets: schematic illustrations of energy band diagrams with reverse biased and forward biased conditions, respectively.

the MWCNTs are functionalized during the electrochemical polymerization of the P3HT material, and the π-conjugation length of the P3HT is reduced. From the results of Raman, UV−vis absorption, PL, and FT-IR spectra, the hybridization of the MWCNTs coated with the P3HT is confirmed.

Nanoscale *I*−*V* Characteristics in the Dark. Figure 4 shows the *I*−*V* characteristic curves of a single strand of a NT in the dark condition at room temperature (RT). The SEM image and its magnification shown in Figure 4a and its inset, respectively, indicate a single strand of the P3HT/MWCNT hybrid NT with Au/Ti four-electrodes. The *I*−*V* characteristic curve for the outer P3HT single NT in the hybrid NT shows semiconducting behavior, while an ohmic behavior is observed for the inner single MWCNT, as shown in Figure 4b. From the slope of the *I*−*V* curves for the MWCNT, the conductivity of the single MWCNT is estimated to be 10^3∼10^4 S/cm. The current level of the P3HT NT is much smaller than that of the MWCNT, but slightly larger than that of the electrochemically synthesized P3HT NW, which was reported earlier.[22] Therefore, we found that chemical treatments and E-beam lithography during the device fabrication do not largely affect the electrical property of the P3HT NT and the MWCNT.

When two electrodes are separately contacted on the MWCNT and the P3HT NT parts, the *I*−*V* characteristic curve of the single strand of P3HT/MWCNT hybrid NT shows a rectification behavior (*i.e.*, nanorectifier) due to the formation of the hybrid junction between the MWCNT and the semiconducting P3HT NT. The insets in Figure 4b show the energy band diagrams to explain this rectification behavior under the forward and reversed bias conditions. The highest occupied molecular orbital (HOMO) and the lowest unoccupied molecular orbital (LUMO) of the P3HT material are 5.2 and 3.0 eV, respectively.[37] The work functions of the oxidized MWCNT and the Au electrode are 4.4 and 5.1 eV, respectively.[38] With a forward bias, the hole carriers are injected from the Au electrode into the *p*-type P3HT NT due to the low energy barrier (≅0.1 eV). The injected holes are easily transported to the MWCNT part by passing through the P3HT NT, as shown in the bottom inset of Figure 4b. With a reverse bias, the hole carriers are injected from the MWCNT into the P3HT NT but it is relatively difficult for the holes to overcome the high energy barrier (≅0.8 eV) between the P3HT NT and the MWCNT at the low bias region ($|V| \leq 1$ V). This gives rise to the observed rectification behavior, which is due to these energy barrier differences so that a single strand of P3HT/MWCNT hybrid NT exhibits well-defined diode characteristics in the coaxial-type p−n hybrid NT structure.

The observed *I*−*V* characteristics of the NTs, under conditions of darkness, can be analyzed through different charge transport mechanisms, as shown in Figure 5. Figure 5a shows a log−log plot of the *I*−*V* curves of the P3HT single NT obtained from the electrical contacts on the outer shell (*i.e.*, the P3HT part) of the P3HT/MWCNT hybrid NT. Two different regimes are observed for the charge transportation, namely that the current increases linearly at low-biasing values ($I \propto V$ for $|V| \leq$ 0.3 V) and the current increases quadratically at high-biasing values ($I \propto V^2$ for $|V| \geq 0.3$ V). In the ohmic region ($|V| \leq 0.3$ V) for the P3HT NT, the current is dominated by thermally generated free carriers, and for $|V| \geq$ 0.3 V the behavior of the current is $I \propto V^2$ representing a space charge limited current (SCLC) model; this suggests that the injected excess carriers from the electrode are relatively large compared with the free carriers of the P3HT NT.[39,40]

The charge transport mechanism for p−n junction structures can be explained using the Fowler-Nordheim tunneling model; $I \propto F^2\exp(-\kappa/F)$, where F is the electric-field strength, and κ is the parameter depending on the barrier shape and height.[41] Figure 5b shows the *I*−*V* characteristic curves of the hybrid junction of the P3HT/MWCNT NT, based on the Fowler−Nordheim tunneling model [$\ln(I/V^2)$ *vs* $1/V$]. The *I*−*V* curves of the P3HT/MWCNT hybrid NT are followed by the Fowler−Nordheim tunneling model at high biasing values ($1/|V| \leq 3$ V^{-1}), (Figure 5b and its inset) which suggests the charge tunneling through triangular barriers, between the P3HT and the electrode for the forward bias condition, and between the P3HT and the MWCNT

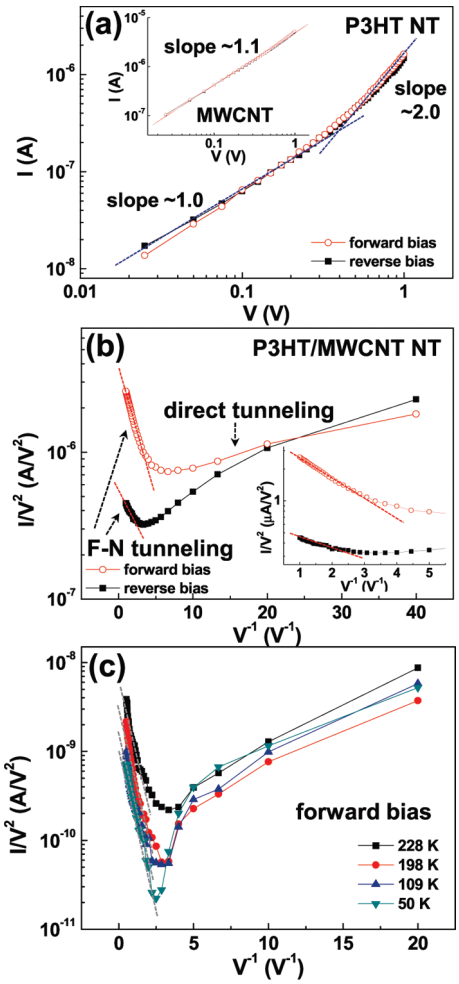

Figure 5. (a) A log−log plot for the *I*−*V* curve of the P3HT NT. Inset: log−log plot for the *I*−*V* curve of the MWCNT. (b) *I*−*V* characteristic curves of the P3HT/MWCNT hybrid NT with forward bias (○) and reverse bias (■), based on the Fowler−Nordheim tunneling model. Inset: magnification of the *I*−*V* characteristic curve at high bias regime ($1/|V| \leq 5$ V^{-1}). (c) Temperature dependence of the *I*−*V* characteristic curves of the P3HT/MWCNT single NT at 228, 198, 109, and 50 K based on the Fowler−Nordheim tunneling model.

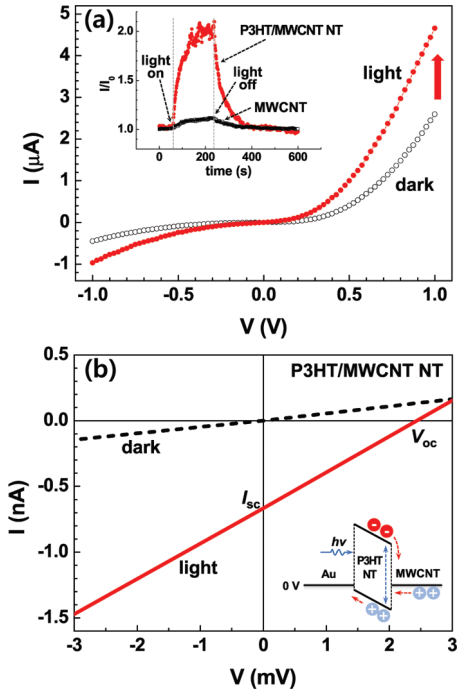

Figure 6. (a) Comparison of the *I*−*V* characteristic curves of the P3HT/MWCNT hybrid NT with (●) and without (○) light illumination. Inset: comparison of the normalized currents of the P3HT/MWCNT hybrid NT (●) and the MWCNT (□) with and without light illumination, as a function of time. (b) *I*−*V* characteristic curves representing a quasi-photovoltaic effect with and without light illumination for a single strand of the P3HT/MWCNT hybrid NT. Inset: schematic illustration of energy band diagram of the hybrid NT to explain quasi-photovoltaic effect.

for the reverse bias situation. In the low bias state, the direct tunneling behaviors[42] [$\ln(I/V^2) \propto \ln(1/V)$] are observed as shown in Figure 5b, because the applied bias is too weak to overcome the barrier height, and the thickness of the P3HT layer is relatively thin as ~20 nm. The observed transition from the direct tunneling to the Fowler−Nordheim tunnelling in Figure 5b has been reported for the junction structure with a low and thin energy barrier, such as in the case of a metal−molecule−metal hybrid junction.[42] With forward biasing, holes are easily tunnelled through the low energy barrier of 0.1 eV between the electrode and the P3HT NT, but in the reverse bias case, holes must be tunnelled through the high energy barrier of 0.8 eV between the MWCNT and the P3HT NT. To confirm the tunneling analysis, temperature dependence of the *I*−*V* curves is measured for the P3HT/MWCNT single NT. Figure 5c shows the *I*−*V* characteristic curves of the P3HT/MWCNT single NT at different temperatures as 228, 198, 109, and 50 K. The current levels slightly decrease with decreasing temperature. The measured *I*−*V* characteristics at low temperatures show the similar transition from the direct tunneling to the Fowler−Nordheim tunneling, as shown in Figure 5c.[43] The rectification effect for the hybrid P3HT/MWCNT single NT can originate from the temperature independent tunneling behavior.

Nanoscale Photoresponsive *I*−*V* Characteristics. Figure 6a presents the photoresponsive *I*−*V* characteristics of the P3HT/MWCNT hybrid single NT. Under light illumination (100 mW/cm^2), the *I*−*V* characteristics of the P3HT/MWCNT hybrid NT also show the rectification behavior. The current levels of the hybrid single NT are clearly enhanced through the light irradiation as shown in Figure 6a. The increased ratio of the current levels, with and without the light illumination, is estimated to be ~2.2 at −1 V and ~1.8 at 1 V. The increase in the current level of the P3HT/MWCNT hybrid NT through the illumination is relatively higher than that of the MWCNT, as shown in the inset of Figure 6a. When the light is incident on the P3HT/MWCNT hybrid NT, the excitons are created in the outer P3HT NT part, which are dissociated to electrons and holes by the applied electric field. The dissociated holes and electrons are transported along the *p*-type P3HT NT and the relative

n-type MWCNT, respectively. These photogenerated carriers and their transportation contribute to the enhancement of the current of the P3HT/MWCNT hybrid NT under the light illumination case so that the photoenhanced nanoscale rectification effect is observed. As shown in the inset of Figure 6a, the decay of photocurrent for the P3HT/MWCNT hybrid NT shows a slow relaxation (*i.e.*, relatively long relaxation time), which is fitted to a single exponential decay of the photocurrent after turning-off the light (see Supporting Information). The observed single exponential decay of the photocurrent suggests charging and discharging of a photogeneraterd single charge carrier through a single photoactive trap.[44−46] Therefore, the photocurrent of the P3HT/MWCNT hybrid NT is caused by single photoactive traps and single charge carriers at the interface. The use of high crystalline organic semiconductors with low trap density and thicker layer for the coaxial-type hybrid NT can improve the switching speed of the photocurrent.[47]

In the p−n junction, the excitons can be dissociated without applied electric field due to the local electric field formed at the junction interface. The difference in the work functions of the electrodes contacting on *p*-type and *n*-type semiconductors can induce the electric field across the p−n junction, which also contributes to the dissociation of the excitons; this is the photovoltaic effect. Figure 6b shows the quasi-photovoltaic effect (*i.e.*, the linear increase of the photocurrent with the applied biasing) measured in the P3HT/MWCNT hybrid single NT. When the applied bias is 0 V, the excitons in the P3HT NT with light irradiation are moved to the junction interface and are dissociated because of both the local electric field formed at the junction interface and the electric field formed by the tilted HOMO and LUMO energy levels due to the difference of the work functions of the Au and the MWCNT materials, as shown in the inset (energy band diagram) of Figure 6b. The dissociated electrons and holes are transported along the MWCNT and the P3HT NT, respectively. The formed equipotential surface in the axial direction of the NTs can effectively assist the charge transport of the dissociated charges.[9,10] The power (*P*) conversion efficiency (η) of PV cells is given by $\eta = FF I_{sc} V_{oc}/P_{in}$,[48] where the fill factor, FF is defined as $FF \equiv I_{max} V_{max}/I_{sc} V_{oc}$. In the experiments, the short circuit current (I_{sc}) is measured to be −0.67 nA, and the open circuit voltage (V_{oc}) is measured to be 2.44 mV. The I_{max} and V_{max} are the current and voltage for the maximum power output, respectively, which can be obtained from $dP/dV = 0$. The I_{max} and V_{max} of the P3HT/MWCNT hybrid NT are estimated to be −0.40 nA and 0.99 mV, respectively, and the FF of the P3HT/MWCNT hybrid NT is estimated to be 0.24, when the P_{in} (input power) is 100 mW/cm^2.

The η of the P3HT/MWCNT hybrid single NT is estimated to be ∼0.42%. For the P3HT/MWCNT hybrid single NT, the current increases linearly near $V = 0$ V under illumination, as shown in Figure 6b, giving the so-called quasi-PV effect. This linear $I-V$ characteristic near $V = 0$ V reduces the FF compared with that of conventional OPV cells having a relatively higher η. The linear PV effect of the P3HT/MWCNT hybrid NT might originate from the thin thickness (∼20 nm) of the P3HT NT and the variation of the work function due to the oxidation of the MWCNTs. For the low reverse bias state, the linear PV effect near $V = 0$ V can be possible through direct tunneling from the MWCNT to the P3HT NT due to the thin thickness of the P3HT NT layer. This analysis is supported by the direct tunneling mechanism in the $I-V$ characteristic curve in low biasing conditions for the hybrid NT in darkness (Figure 5b). From the FT-IR spectra, it is observed that the MWCNT of the hybrid NT is functionalized during the electrochemical polymerization of the P3HT materials, resulting in the increase of the work function of the MWCNT.[31] For the P3HT/MWCNT hybrid NT, the difference of the work functions for the functionalized MWCNT and the Au electrode is reduced, and the flat band voltage and V_{oc} are considerably decreased so that a linear PV effect is observed in the low forward biased region. It is suggested that, when the fullerene derivatives, such as [6,6]-phenyl-C_{61}-butyric acid methyl ester (PCBM), with *n*-type characteristics are inserted between the MWCNT and the P3HT NT, the typical $I-V$ characteristic curves of the OPV cells can be observable with high η.

CONCLUSION

Coaxial-type hybrid NTs consisting of the MWCNT coated with light-emitting P3HT material have been fabricated. The P3HT/MWCNT hybrid NTs have been characterized through HR-TEM, Raman, UV−vis absorption, FT-IR, and PL experiments. The PL intensity of the P3HT materials decreases after the hybridization with the MWCNT due to the charge transfer effect. The $I-V$ characteristics show the semiconducting behavior for the outer P3HT NT and an ohmic behavior for the inner MWCNT. The $I-V$ characteristics of the hybrid junction between the outer P3HT NT and the inner MWCNT show a rectification behavior, whose efficiency is clearly enhanced with light irradiation; that is, a photoenhanced nanoscale rectification effect. The rectification effect has been analyzed through the combination of the Fowler−Nordheim tunneling model and direct charge tunneling model. The quasi-photovoltaic effect in the single strand of the P3HT/MWCNT hybrid NT has been observed.

EXPERIMENTAL SECTION

MWCNT Growth. MWCNTs have been grown by a conventional thermal CVD method and a 5 nm-thick Fe film is deposited on a SiO_2 (200 nm)/*n*-Si substrate using an electron beam (E-beam) evaporator under a pressure of 10^{-6} Torr. The catalyst deposited substrates are loaded on a quartz boat and Ar (1000 sccm) is allowed to flow into a quartz CVD reactor to prevent the oxidation of the catalyst metal while raising the temperature. The catalyst films are pretreated by H_2 gas with a flow rate of 30 sccm for 5 min at 750 °C and then C_2H_4 (30 sccm) and Ar (100 sccm)

are allowed to flow into the quartz reactor for 10 min at the same temperature. After growing the MWCNT, the reactor is cooled down to RT under an Ar ambient.

Fabrication of Hybrid P3HT/MWCNT NTs. For the electrochemical polymerization of the P3HT material onto the MWCNT, the molar ratio of the 3-HT monomer to the $BMIMPF_6$ ionic liquid is 5:1. The 3-HT monomers and the $BMIMPF_6$ have been purchased from Sigma-Aldrich Co., and these are used without further purification. For the polymerization of the 3-HT monomers, a constant voltage of 4.3 V is applied for 90 s to obtain a uniform and relatively thick P3HT layer onto the MWCNT, and the measured current density between electodes is 1.6 mA/cm^2.[22] The P3HT/MWCNT hybrid NTs are dried in a vacuum for 30 min after rinsing with methanol. The P3HT/MWCNT hybrid NTs scratched from the SiO_2/*n*-Si substrate by using a razor are dispersed in methanol solvent.

Fabrication of P3HT NTs. The P3HT NTs themselves as a reference material are electrochemically synthesized by using an Al_2O_3 nanoporous template with pore size of 100 nm (Whatman International Ltd.), as previously reported.[22] The electrolyte is consisted of 3-HT monomers, $BMIMPF_6$ ionic liquid, and anhydrous acetonitrile (CH_3CN) as a solvent. The molar ratio of the 3-HT monomer to the $BMIMPF_6$ ionic liquid is 5:1. The constant voltage within 4.5−5.0 V range is applied to the electrode for the polymerization for 8 min, and the measured current density between electrodes is ~1.4 mA/cm^2. The Al_2O_3 nanoporous template is removed by using either 2.0 M HF or 2.0 M NaOH solvent. The resulting P3HT NTs are dipersed in methanol after removal of the Al_2O_3 nanoporous template only.

Measurements. The *I*−*V* characteristic curves of the NTs are measured under a vacuum condition of below 10^{-3} Torr, using Keithley 237 SMU and Keithley 487 picoammeter instruments. The CTI-cryogenic cryostat system is used to measure the temperature dependence of the *I*−*V* characteristic curves for the P3HT/MWCNT hybrid NT. The incident light power from a mercury−xenon lamp (Spectra-Physics 66902) is 100 mW/cm^2, measured by using an optical power meter (Thorlabs PM120) connected to a sensor (Thorlabs S130A) at the sample location, and the distance between the device and the light source is ~30 cm. The leakage current could be neglected due to its relatively low level of less than 1 nA, with or without the light illumination. For the SEM and the HR-TEM images, the Hitachi S-4300 and JEOL JEM-3010 systems are used, respectively. The optical properties of the NTs dispersed in chloroform ($CHCl_3$) solution are analyzed through ultraviolet and visible (UV−vis) absorption (Agilent 8453) and the photoluminescence (PL; Hitachi F-7000) spectra. For the structural properties, Raman (Horiba Jobin-Yvon, HR-800 UV, Ar^+ laser excitation, laser beam wavelength = 514.5 nm) and FT-IR (Thermo Electron Corporation, Nicolet 380) spectra are measured. For measuring the Φ_{QY} of the P3HT NTs dispersed in $CHCl_3$ solution, the excitation wavelength is 410 nm. As a standard material for the measurement of Φ_{QY}, Coumarin 153 dissolved in ethanol (Φ_{QY} = 0.38) is used.[49] The Φ_{QY} for electrochemically synthesized P3HT NTs has been obtained from $\Phi_{QY} = \Phi_{st}$ ($Grad_x/Grad_{st}$) (β_x^2/β_{st}^2).[50] Here, the subscripts, st and *x*, denote the standard sample and the measured NTs, respectively. Grad means the gradient of the plot of the integrated fluorescence intensity *versus* absorbance. The β is the refractive index of the solution.

Acknowledgment. This work was supported by a National Research Foundation of Korea (NRF) grant funded by the Korean government (MEST) (Grant No. R0A-2007-000-20053-0).

Supporting Information Available: FT-IR, Raman spectra, and the photocurrent analysis of P3HT/MWCNT hybrid coaxial NTs; quantum yields (Φ_{QY}) of the P3HT NTs. This material is available free of charge *via* the Internet at http://pubs.acs.org.

REFERENCES AND NOTES

1. Forrest, S. R. The Path to Ubiquitous and Low-Cost Organic Electronic Appliances on Plastic. *Nature* **2004**, *428*, 911–918.
2. Yu, G.; Pakbaz, K.; Heeger, A. J. Semiconducting Polymer Diodes: Large Size, Low Cost Photodetectors with Excellent Visible−Ultraviolet Sensitivity. *Appl. Phys. Lett.* **1994**, *64*, 3422–3424.
3. Cho, M. Y.; Kim, S. J.; Han, Y. D.; Park, D. H.; Kim, K. H.; Choi, D. H.; Joo, J. Highly Sensitive, Photocontrolled, Organic Thin-Film Transistors Using Soluble Star-Shaped Conjugated Molecules. *Adv. Funct. Mater.* **2008**, *18*, 2905–2912.
4. Li, G.; Shrotriya, V.; Huang, J.; Yao, Y.; Moriarty, T.; Emery, K.; Yang, Y. High-Efficiency Solution Processable Polymer Photovoltaic Cells by Self-Organization of Polymer Blends. *Nat. Mater.* **2005**, *4*, 864–868.
5. Park, S. H.; Roy, A.; Beaupré, S.; Cho, S.; Coates, N.; Moon, J. S.; Moses, D.; Leclerc, M.; Lee, K.; Heeger, A. J. Bulk Heterojunction Solar Cells with Internal Quantum Efficiency Approaching 100%. *Nat. Photonics* **2009**, *3*, 297–302.
6. Huang, Y.; Duan, X.; Cui, Y.; Lauhon, L. J.; Kim, K. -H.; Lieber, C. M. Logic Gates and Computation from Assembled Nanowire Building Blocks. *Science* **2001**, *294*, 1313–1317.
7. Lee, J. U.; Gipp, P. P.; Heller, C. M. Carbon Nanotube p−n Junction Diodes. *Appl. Phys. Lett.* **2004**, *85*, 145–147.
8. Lee, J. U. Photovoltaic Effect in Ideal Carbon Nanotube Diodes. *Appl. Phys. Lett.* **2005**, *87*, 073101.
9. Tian, B.; Zheng, X.; Kempa, T. J.; Fang, Y.; Yu, N.; Yu, G.; Huang, J.; Lieber, C. M. Coaxial Silicon Nanowires as Solar Cells and Nanoelectronic Power Sources. *Nature* **2007**, *449*, 885–889.
10. Kayes, B. M.; Atwater, H. A.; Lewis, N. S. Comparison of the Device Physics Principles of Planar and Radial p−n Junction Nanorod Solar Cells. *J. Appl. Phys.* **2005**, *97*, 114302.
11. Nduwimana, A.; Wang, X. -Q. Charge Carrier Separation in Modulation Doped Coaxial Semiconductor Nanowires. *Nano Lett.* **2009**, *9*, 283–286.
12. Tian, B.; Kempa, T. J.; Lieber, C. M. Single Nanowire Photovoltaics. *Chem. Soc. Rev.* **2009**, *38*, 16–24.
13. Guldi, D. M.; Rahman, G. M. A.; Zerbetto, F.; Prato, M. Carbon Nanotubes in Electron Donor−Acceptor Nanocomposites. *Acc. Chem. Res.* **2005**, *38*, 871–878.
14. Geng, J.; Kong, B. -S.; Yang, S. B.; Youn, S. C.; Park, S.; Joo, T.; Jung, H. -T. Effect of SWNT Defects on the Electron Transfer Properties in P3HT/SWNT Hybrid Materials. *Adv. Funct. Mater.* **2008**, *18*, 2659–2665.
15. Sgobba, V.; Guldi, D. M. Carbon Nanotubes as Integrative Materials for Organic Photovoltaic Devices. *J. Mater. Chem.* **2008**, *18*, 153–157.
16. Günes, S.; Neugebauer, H.; Sariciftci, N. S. Conjugated Polymer-Based Organic Solar Cells. *Chem. Rev.* **2007**, *107*, 1324–1338.
17. Bao, Z.; Dodabalapur, A.; Lovinger, A. J. Soluble and Processable Regioregular Poly(3-hexylthiophene) for Thin Film Field-Effect Transistor Applications with High Mobility. *Appl. Phys. Lett.* **1996**, *69*, 4108–4110.
18. Greenham, N. C.; Brown, A. R.; Bradley, D. D. C.; Friend, R. H. Electroluminescence in Poly(3-alkylthienylene)s. *Synth. Met.* **1993**, *55*−*57*, 4134–4138.
19. Kim, J. Y.; Lee, K.; Coates, N. E.; Moses, D.; Nguyen, T. -Q.; Dante, M.; Heeger, A. J. Efficient Tandem Polymer Solar Cells Fabricated by All-Solution Processing. *Science* **2007**, *317*, 222–225.
20. Briseno, A. L.; Holcombe, T. W.; Boukai, A. I.; Garnett, E. C.; Shelton, S. W.; Fréchet, J. J. M.; Yang, P. Oligo- and Polythiophene/ZnO Hybrid Nanowire Solar Cells. *Nano Lett.* **2010**, *10*, 334–340.
21. Ratcliff, E. L.; Jenkins, J. L.; Nebesny, K.; Armstrong, N. R. Electrodeposited, "Textured" Poly(3-hexyl-thiophene) (e-P3HT) Films for Photovoltaic Applications. *Chem. Mater.* **2008**, *20*, 5796–5806.
22. Lee, S. H.; Park, D. H.; Kim, K.; Joo, J. Confocal Microscope Photoluminescence and Electrical Characteristics of Single Poly(3-hexylthiophene) Nanowire Strand. *Appl. Phys. Lett.* **2007**, *91*, 263102.
23. Baibarac, M.; Lapkowski, M.; Pron, A.; Lefrant, S.; Baltog, I. SERS Spectra of Poly(3-hexylthiophene) in Oxidized and Unoxidized States. *J. Raman Spectrosc.* **1998**, *29*, 825–832.

24. Nii, H.; Sumiyama, Y.; Nakagawa, H.; Kunishige, A. Influence of Diameter on the Raman Spectra of Multiwalled Carbon Nanotubes. *Appl. Phys. Express* **2008**, *1*, 064005.
25. Zhang, D.; Kandadai, M. A.; Cech, J.; Roth, S.; Curran, S. A. Poly(L-lactide) (PLLA)/Multiwalled Carbon Nanotube (MWCNT) Composite: Characterization and Biocompatibility Evaluation. *J. Phys. Chem. B* **2006**, *110*, 12910–12915.
26. Zhao, Q.; Wagner, H. D. Raman Spectroscopy of Carbon-Nanotube-Based Composites. *Philos. Trans. R. Soc., A* **2004**, *362*, 2407–2424.
27. Yu, J.; Grossiord, N.; Koning, C. E.; Loos, J. Controlling the Dispersion of Multiwall Carbon Nanotubes in Aqueous Surfactant Solution. *Carbon* **2007**, *45*, 618–623.
28. Chen, T. -A.; Wu, X.; Rieke, R. D. Regiocontrolled Synthesis of Poly(3-alkylthiophenes) Mediated by Rieke Zinc: Their Characterization and Solid-State Properties. *J. Am. Chem. Soc.* **1995**, *117*, 233–244.
29. Arranz-Andrés, J.; Blau, W. J. Enhanced Device Performance Using Different Carbon Nanotube Types in Polymer Photovoltaic Devices. *Carbon* **2008**, *46*, 2067–2075.
30. Patil, A. O.; Heeger, A. J.; Wudl, F. Optical Properties of Conducting Polymers. *Chem. Rev.* **1988**, *88*, 183–200.
31. Berson, S.; De Bettignies, R.; Bailly, S.; Guillerez, S.; Jousselme, B. Elaboration of P3HT/CNT/PCBM Composites for Organic Photovoltaic Cells. *Adv. Funct. Mater.* **2007**, *17*, 3363–3370.
32. Rogers, R. D.; Seddon, K. R. Ionic Liquids—Solvents of the Future. *Science* **2003**, *302*, 792–793.
33. Lu, W.; Fadeev, A. G.; Qi, B.; Smela, E.; Mattes, B. R.; Ding, J.; Spinks, G. M.; Mazurkiewicz, J.; Zhou, D.; Wallace, G. G.; *et al*. Use of Ionic Liquids for π-Conjugated Polymer Electrochemical Devices. *Science* **2002**, *297*, 983–987.
34. Wasserscheid, P.; Keim, W. Ionic Liquids—New "Solutions" for Transition Metal Catalysis. *Angew. Chem., Int. Ed.* **2000**, *39*, 3772–3789.
35. Khatri, I.; Adhikari, S.; Aryal, H. R.; Soga, T.; Jimbo, T.; Umeno, M. Improving Photovoltaic Properties by Incorporating Both Single Walled Carbon Nanotubes and Functionalized Multiwalled Carbon Nanotubes. *Appl. Phys. Lett.* **2009**, *94*, 093509.
36. Shanmugharaj, A. M.; Bae, J. H.; Nayak, R. R.; Ryu, S. H. Preparation of Poly(styrene-*co*-acrylonitrile)-Grafted Multiwalled Carbon Nanotubes *via* Surface-Initiated Atom Transfer Radical Polymerization. *J. Polym. Sci., Polym. Chem.* **2007**, *45*, 460–470.
37. Onoda, M.; Tada, K.; Zakhidov, A. A.; Yoshino, K. Photoinduced Charge Separation in Photovoltaic Cell with Heterojunction of p- and n-type Conjugated Polymers. *Thin Solid Films* **1998**, *331*, 76–81.
38. Ago, H.; Kugler, T.; Cacialli, F.; Salaneck, W. R.; Shaffer, M. S. P.; Windle, A. H.; Friend, R. H. Work Functions and Surface Functional Groups of Multiwall Carbon Nanotubes. *J. Phys. Chem. B* **1999**, *103*, 8116–8121.
39. Lampert, M. A. Simplified Theory of Space-Charge-Limited Currents in an Insulator with Traps. *Phys. Rev.* **1956**, *103*, 1648–1656.
40. Kao, K. C.; Hwang, W. *Electrical Transport in Solids*, Pergamons; New York, 1981.
41. Parker, I. D. Carrier Tunneling and Device Characteristics in Polymer Light-Emitting Diodes. *J. Appl. Phys.* **1994**, *75*, 1656–1666.
42. Beebe, J. M.; Kim, B. S.; Gadzuk, J. W.; Frisbie, C. D.; Kushmerick, J. G. Transition from Direct Tunneling to Field Emission in Metal−Molecule−Metal Junctions. *Phys. Rev. Lett.* **2006**, *97*, 026801.
43. Pakoulev, A. V.; Burtman, V. Temperature Dependent Barrier Crossover Regime in Tunneling Single Molecular Devices Based on the Matrix of Isolated Molecules. *J. Phys. Chem. C* **2009**, *113*, 21413–21421.
44. Vaveliuk, P.; Ruiz, B.; Bolognini, N. Theoretical Analysis of the Photocurrent Dark Decay in Photorefractive Media. *IEEE J. Quantum Electron.* **2000**, *36*, 692–697.
45. Balland, J. C.; Zielinger, J. P.; Noguet, C.; Tapiero, M. Investigation of Deep Levels in High-Resistivity Bulk Materials by Photoinduced Current Transient Spectroscopy: I. Review and Analysis of Some Basic Problems. *J. Phys. D, Appl. Phys* **1986**, *19*, 57–70.
46. Hippel, A.; Gross, E. P.; Jelatis, J. G.; Geller, M. Photocurrent, Space-Charge Buildup, and Field Emission in Alkali Halide Crystals. *Phys. Rev.* **1953**, *91*, 568–579.
47. Hwang, I.; McNeill, C. R.; Greenham, N. C. Drift-Diffusion Modeling of Photocurrent Transients in Bulk Heterojunction Solar Cells. *J. Appl. Phys.* **2009**, *106*, 094506.
48. Sze, S. M. *Physics of Semiconductor Devices*, 2nd ed.; John Wiley & Sons, Inc.: New York, 1981.
49. Jones, G.; Rahman, M. A. Fluorescence Properties of Coumarin Laser Dyes in Aqueous Polymer Media. Chromophore Isolation in Poly(methacrylic acid) Hypercoils. *J. Phys. Chem.* **1994**, *98*, 13028–13037.
50. Williams, A. T. R.; Winfield, S. A.; Miller, J. N. Relative Fluorescence Quantum Yields Using a Computer-Controlled Luminescence Spectrometer. *Analyst* **1983**, *108*, 1067–1071.